AMMRC TR 80-19

STRENGTH DEGRADATION OF ARAMID-FIBER/EPOXY COMPOSITES

APRIL 1980

EDWARD M. WU
WASHINGTON UNIVERSITY
MATERIALS RESEARCH LABORATORY
ST. LOUIS, MO 63130

FINAL REPORT

CONTRACT NUMBER DAAG46-75-C-0081

Prepared for

ARMY MATERIALS AND MECHANICS RESEARCH CENTER
Watertown, Massachusetts 02172

The findings in this report are not to be construed as an official Department of the Army position, unless so designated by other authorized documents.

Mention of any trade names or manufacturers in this report shall not be construed as advertising nor as an official indorsement or approval of such products or companies by the United States Government.

DISPOSITION INSTRUCTIONS

Destroy this report when it is no longer needed.
Do not return it to the originator.

Unclassified

SECURITY CLASSIFICATION OF THIS PAGE (When Data Entered)

REPORT DOCUMENTATION PAGE

READ INSTRUCTIONS BEFORE COMPLETING FORM

1. REPORT NUMBER: AMMRC TR-80-19	2. GOVT ACCESSION NO.: AD-A085670
3. RECIPIENT'S CATALOG NUMBER:	
4. TITLE (and Subtitle): STRENGTH DEGRADATION OF ARAMID-FIBER/EPOXY COMPOSITES	5. TYPE OF REPORT & PERIOD COVERED: Final Report
	6. PERFORMING ORG. REPORT NUMBER:
7. AUTHOR(s): EDWARD M. WU	8. CONTRACT OR GRANT NUMBER(s): DAAG46-75-C-0081
9. PERFORMING ORGANIZATION NAME AND ADDRESS: WASHINGTON UNIVERSITY MATERIALS RESEARCH LABORATORY ST. LOUIS, MO 63130	10. PROGRAM ELEMENT, PROJECT, TASK AREA & WORK UNIT NUMBERS: D/A Proj: 1T162105AH84 AMCMS CODE: 612105.11.H84 Agency Acc No: DA0B4757
11. CONTROLLING OFFICE NAME AND ADDRESS: ARMY MATERIALS & MECHANICS RESEARCH CENTER WATERTOWN, MASSACHUSETTS 02172	12. REPORT DATE: April 1980 13. NUMBER OF PAGES: 12 150
14. MONITORING AGENCY NAME & ADDRESS (if different from Controlling Office)	15. SECURITY CLASS. (of this report): Unclassified
	15a. DECLASSIFICATION/DOWNGRADING SCHEDULE: N/A

16. DISTRIBUTION STATEMENT (of this Report)

APPROVED FOR PUBLIC RELEASE; DISTRIBUTION UNLIMITED.

17. DISTRIBUTION STATEMENT (of the abstract entered in Block 20, if different from Report)

18. SUPPLEMENTARY NOTES

19. KEY WORDS (Continue on reverse side if necessary and identify by block number)

COMPOSITE MATERIALS
ARAMID FIBER
KEVLAR
EPOXY LAMINATES
DEGRADATION
APPLIED MECHANICS
MECHANICAL PROPERTIES

20. ABSTRACT (Continue on reverse side if necessary and identify by block number)

The moisture absorption kinetics for Kevlar 49 epoxy have been measured for four environmental conditions. The strength degradation for the composite has been systematically measured by six experiments for each of the four states. The tensor polynomial strength coefficients are generalized to represent the strength degradation for the moisture absorbed states.

(over)

DD FORM 1 JAN 73 1473 EDITION OF 1 NOV 65 IS OBSOLETE

SECURITY CLASSIFICATION OF THIS PAGE (When Data Entered)

20. (continued)

Due to the big difference between tensile and compressive strength for Kevlar 49 composites, analytical representation of the failure surface requires a third-order tensor polynomial. Four additional biaxial experiments are needed to provide the necessary data. The degree of fiber-controlled strength degradation is different from the degradation of matrix-controlled strength, which causes the failure surface to shift and deform. This shift should also be characterized by a third-order tensor polynomial.

SUMMARY

The moisture absorption kinetics for Kevlar 49 epoxy have been measured for four environmental conditions. The strength degradation for the composite has been systematically measured by six experiments for each of the four states. The tensor polynomial strength coefficients are generalized to represent the strength degradation for the moisture absorbed states.

Due to the big difference between tensile and compressive strength for Kevlar 49 composites, analytical representation of the failure surface requires a third-order tensor polynomial. Four additional biaxial experiments are needed to provide the necessary data. The degree of fiber-controlled strength degradation is different from the degradation of matrix-controlled strength, which causes the failure surface to shift and deform. This shift should also be characterized by a third-order tensor polynomial.

TABLE OF CONTENTS

LIST OF ILLUSTRATIONS

LIST OF ILLUSTRATIONS
(continued)

LIST OF TABLES

INTRODUCTION

Strength degradation of composites in the presence of a particular environment is an important parameter in the design and utilization of composites. For polymeric matrix composites, moisture environment is known to cause severe strength degradation (1,2). For Aramid fiber composites, the severity of the strength degradation is further compounded by the fiber's affinity for moisture as well (3). It is thus pertinent to assess the combined effect of the dual moisture absorption of the fiber and matrix.

Since moisture transport into a composite is a kinetic process and swelling stress induces time-dependent strength alteration, a complete characterization of the resultant strength degradation requires a hereditary integration of the stress history and the moisture absorption/desorption history. In principle, this procedure is akin to the hereditary integral in viscoelasticity. In this particular context, we need to develop a general strength degradation function of stress, moisture, and time. As an initial step, we treat the special case in which stress and moisture are taken to be separable in time, i.e. the composite is exposed to moisture in the absence of applied stress (but possibly in the presence of fabrication-induced stress) and the moisture content is postulated to be a state variable affecting the strength.

The Aramid fiber composite characterized herein is Kevlar 49 filament wound with a XD7818/Jeffamine T403 epoxy. This composite is fabricated into plate and tube forms by a filament winding process

(at AMMRC), exposed to three moisture-temperature environment conditions and, upon reaching equilibrium, mechanically tested in six states of loadings to assess the failure envelope as a function of moisture absorption content.

MOISTURE EXPOSURE PROCEDURE

The sample materials consisted of filament-wound plates and tubes. Details of the fabrication procedure are described in Appendix I. Upon receipt, the samples were kept in a desiccated oven at 50°C for 72 hours at atmospheric pressure and subsequently stored in sealed bags with silica gel desiccant. This is the controlled initial dry state (0% moisture). The sample materials were divided into four groups, one control and three groups to be treated under the following conditions:

1. 52% Relative Humidity at 23°C
2. Liquid water at 23°C
3. Liquid water at 100°C (water boil)

The first condition is maintained by a sealed chamber with a saturated solution of sodium dichromate. The second condition is by immersion in distilled water at 23°C, and the third condition is by immersion in liquid boiling distilled water. Moisture absorption is calculated by weighing the samples at appropriate time-intervals. The results of the water absorption under these conditions are presented in Figures 1 and 2 using $\sqrt{(\text{time})}$ to observe the initial Fickian diffusion. Also represented are uncoated Kevlar 49 fibers subjected to comparable conditions (but in

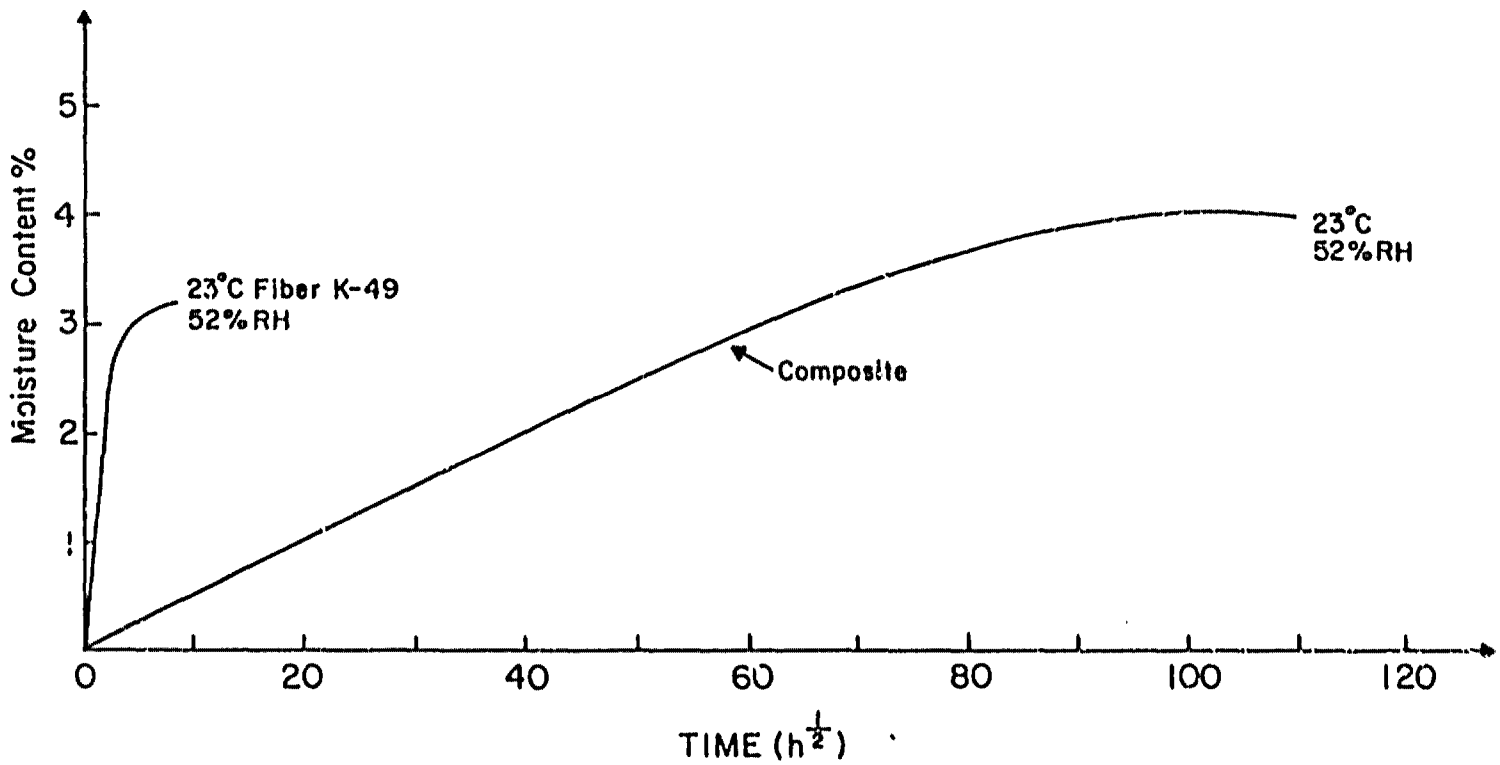

Figure 1. Water absorption rate of kevlar 49 fiber and K-49/epoxy composite at 52% relative humidity and 23°C.

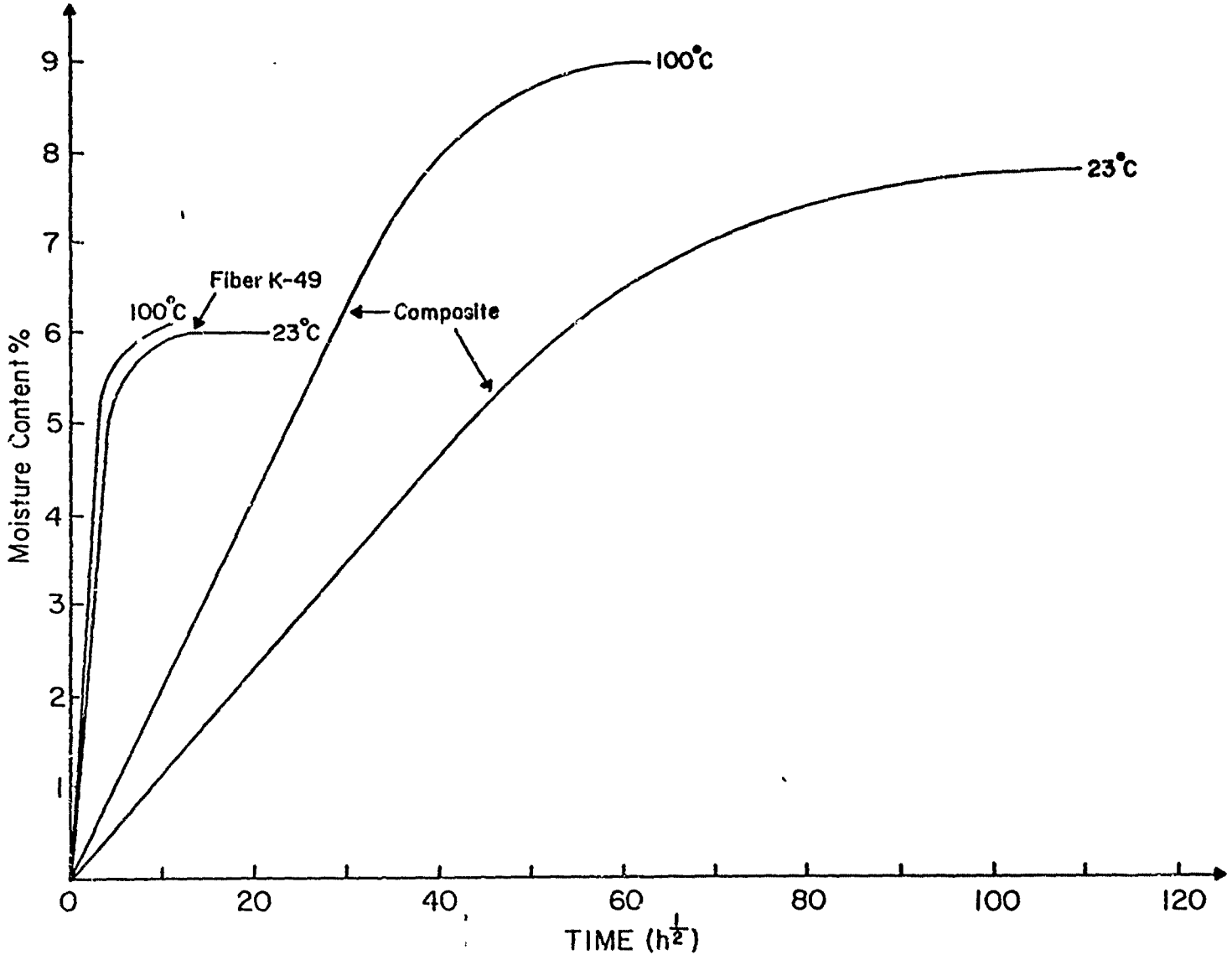

Figure 2. Water absorption rate of Kevlar-49 fiber and K-49/epoxy composite in liquid water at 23°C and 100°C (boiling).

a different apparatus due to the different weight measurement resolution requirements*). The results are summarized in Table 1.

Table 1

Equilibrium Moisture Content % Above Baseline

	52% RH/23°C	Liquid H_2O/23°C	Liquid H_2O/100°C
Kevlar-49 fiber	3.2	6.0	6.1
Kevlar-49/XD-T403	4.1	7.8	8.9
Epoxy XD-T403*	(0.3-5.7)	(5.6-11.0)	(8.5-13.9)

*By difference of fiber and composite moisture content using rule of mixtures with V_f = 58.1%, Density of fiber-1.45 gm/cc, Density of matrix-1.189 gm/cc; void volume fraction is 2.5% (ASTM D2734).

We note from Figures 1 and 2 that because the rate of moisture uptake for the fiber is much faster than that for the epoxy, the moisture absorption rate for the composite is primarily governed by the epoxy-water absorption rate. Secondly, from Table 1 we note that a significant percentage of the moisture is absorbed in the fiber which leads to a degradation of fiber-controlled strengths; this degradation of composite strength in the fiber direction is normally very small for graphite fiber composites but is significant for Kevlar composites. Thirdly, the calculated upper bound moisture contents for the epoxy are higher than those reported for neat

*The nominal weight of the composite samples is 15 grams. The weight of these samples is measured on a balance with a weight resolution of 0.01 gram. The nominal weight of the fiber samples is 0.2 grams. The weight of these samples is measured in a balance with weight resolution of 0.001 gram.

epoxies. This suggests that free water may have accumulated in the voids of the composite, hence the range of possible resin moisture contents shown in Table 1.

The samples were exposed until equilibrium was reached. They were then mechanically tested to evaluate the strength degradation due to the exposure history and the moisture content.

STRENGTH MEASUREMENTS

The objective of the mechanical testing is to assess the effect of absorbed moisture on the strength of the composite under multiaxial loading conditions as normally experienced by the composite in structural applications. In a structure under service loading conditions, different locations of the structure experience various combined-stress ratios. These combined-stress ratios can be graphically represented as rays as depicted schematically (in 2-dimensions-rays a, b, c, etc.) in Figure 3a. The limiting load carried under each of these combined loading conditions determines a point at the end of each ray; the envelope formed by these points defines a failure envelope. Thus, when the failure envelope for a material is known, we can estimate the integrity of a structure under general service loading. The determination of such a failure surface for a Kevlar composite is the objective of this investigation.

The failure envelope for a composite may be obtained through exhaustive testing by varying the combined loading ratios until the entire surface has been mapped out. The experimental effort for such an approach may be estimated. Assume that we vary the loading conditions such that each ray is spaced 30° apart, then to map out a two-dimensional surface requires 360/30 or 12 different tests. However, even for a

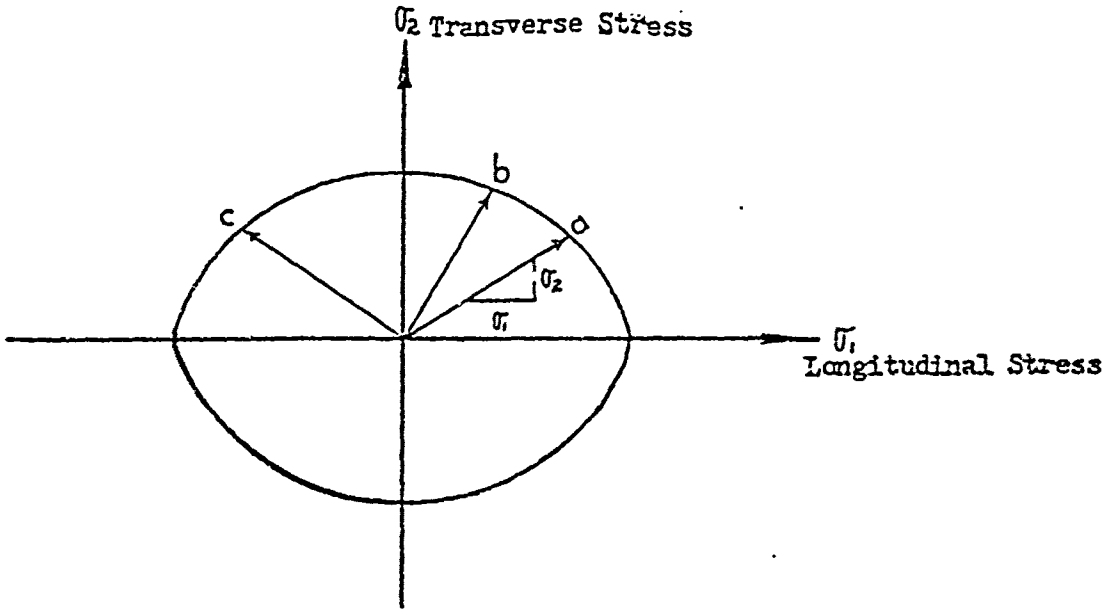

Fig. 3a Two-dimensional schematic of rays representing combined loading ratios terminating to form a failure surface.

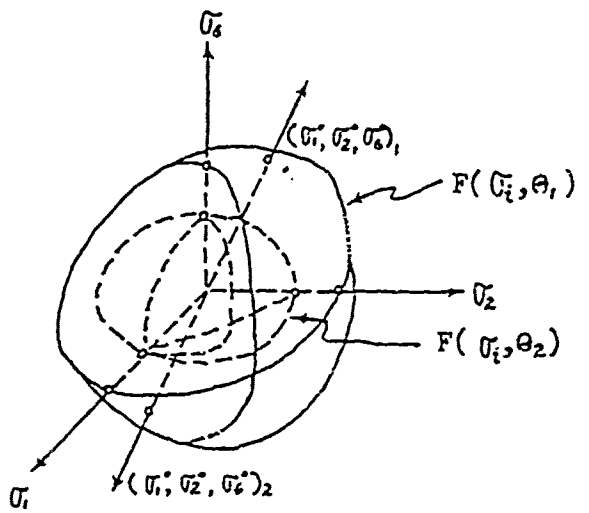

Fig. 3b Schematic of a failure surface.

planar two-dimensional composite, there exist three components of stress; longitudinal, transverse and shear stress. Thus, a three-dimensional surface is needed. If we subdivide such three-dimensional surfaces into 6 planes, then a total of 6 x 12 or 72 tests are required. If each combined loading test is repeated in five replicas, then the total number of measurments is 360. This number has to be multiplied by the different environmental conditions, thus making the task quite substantial.

As an alternative to exhaustive testing and to experimentally trace out a failure surface, we chose to leave the form of the failure criteria general and perform the necessary guiding experiments to define the failure surface. A summary of the current failure criteria and the critical guiding experiments have been presented by Wu (4). The same characterization procedures are used herein. Briefly, a failure criterion is a mathematical representation of a failure surface of a composite in a given state, i.e. at a given temperature, loading rate. environmental history, etc. In such a state $f(\sigma_i,\Theta_1)$, the failure surface is illustrated in Figure 3b where Θ_i is a generalized variable defining the state, e.g. the moisture content. At another state $f(\sigma_i,\Theta_2)$, the failure surface (such as after moisture exposure) can be in general different in size and in shape than the former state. The objective here is to define the shape of the surface with a minimum number of experiments. The experimental strategy may be visualized by considering the most expedient way to establish the function of two variables; i.e., a curve in a two-parameter space. We may initially assume the curve to be a straight line; this requires two tests performed

respectively at the axis-crossing of the two parameters. We may then interrogate whether the curve is second-order, say, a parabola. This requires one additional test at a combined ratio of the two parameters. The result of this third test either confirms or disputes the former assumption that it is a straight line. Further combined tests may be used to interrogate whether the curve is 3rd, 4th or higher order. In other words we are sequentially determining the coefficients of a polynomial until the curve is adequately represented.

Similarly for a three-dimensional failure surface, geometrically (Figure 3b) it is self obvious that we need to determine the axis crossings of the surface. For a planar composite, there exist three stress components, and if the composite strength is symmetrical to shear stress, then there are five independent axis crossings. There can be infinite possibilities of different failure surfaces which possess the same axis crossings; thus, we need a minimum of one additional experiment to define (more uniquely) the shape. These six guiding experiments for determining the failure criterion of a composite are illustrated in Figure 4. The formalism of arriving at these guiding-experiments can be thought of by representing the failure surface as a tensor polynomial and sequentially determining the coefficients of the polynomial:

$$F_i\sigma_i + F_{ij}\sigma_i\sigma_j + \ldots = 1 \qquad (1)$$

The details of the derivation as well as experimental design and testing methods are all reviewed in Reference (4). We will use these procedures

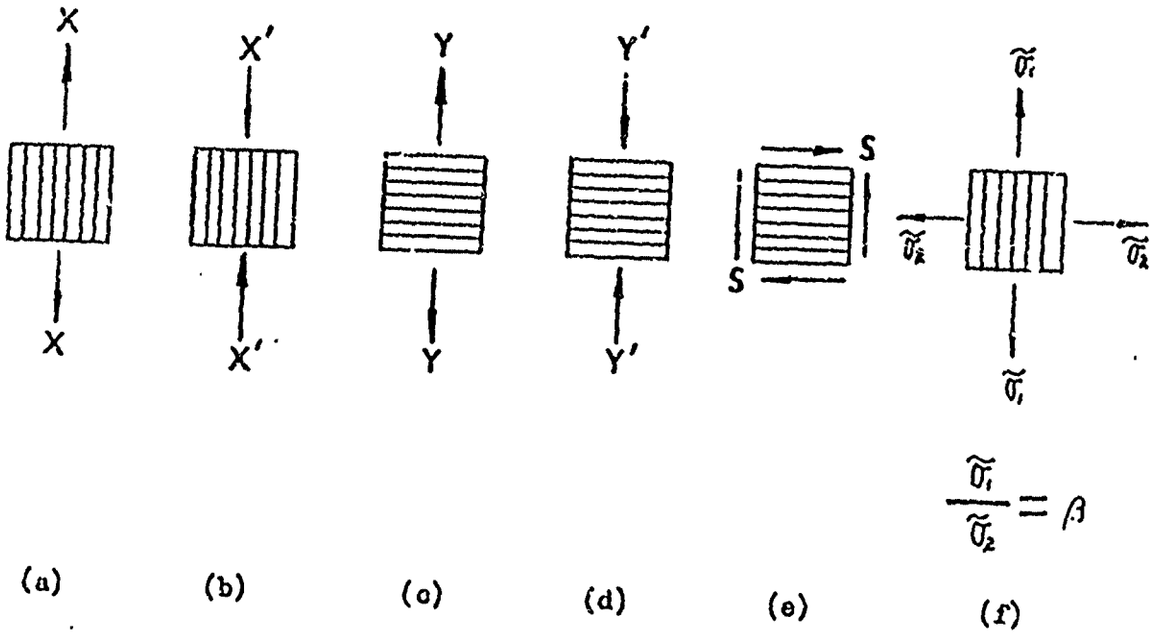

Figure 4. Guiding experiments for characterizing a failure surface.

without further elaboration. Briefly, all tension tests (tests 'a' and 'c') were performed using flat coupons of the conventional 'IITRI' configuration. A picture of the 'IITRI' sample coupon is shown in Figure 5; the detailed dimensions of the samples are specified by ASTM Standard D 3039. Longitudinal compression (test 'b') was performed in a "Celanese" fixture. The "Celanese" fixture transmits compressive force through tabs (to prevent end buckling and brooming) utilizing conical wedges which are guided in a precision cylindrical shell. A picture of such a fixture is shown in Figure 6. Transverse compression (test 'd') was performed on a one-inch (ID), 2-inch long, 0.05-inch thick, hoop-wound tube; the same hoop-wound tube was also used for the shear test. The biaxial test ('f') induced an axial force and internal pressure as described in reference (5). For the series of tube tests using hoop-wound tubes, considerable processing development was required. Originally, the hoop-wound angle deviated from 90° by $\pm$10° as a result of winding passes from left and right. This winding pattern gave rise to excessively high shear strengths. This was subsequently modified by using inding pattern wherein the hoop-wound angle still deviated from 90° by only +5° as a result of passing from only one direction. The details of this process are described in Appendix I. The data reported herein were obtained from samples using this final winding pattern. A total of 37 tubular samples was utilized in the test development of the shear and biaxial tests. Finally, the purpose of the biaxial test (test 'f') is to identify the existence of strength coupling under normal stresses. That is, when both longitudinal and

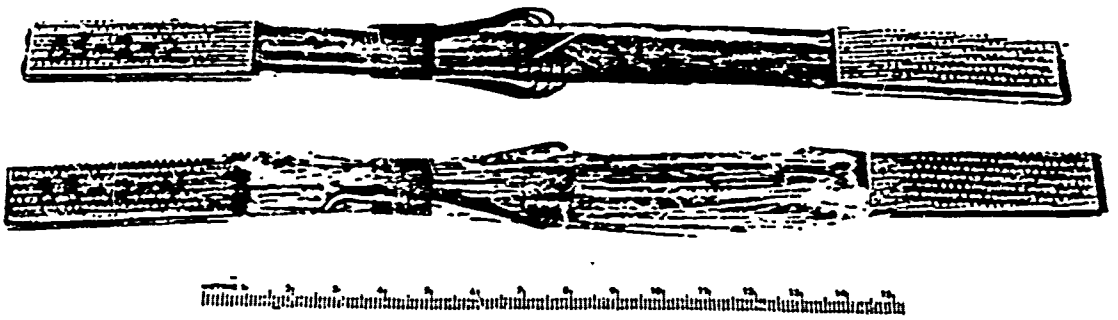

Figure 5. 'IITRI' tensile coupon.

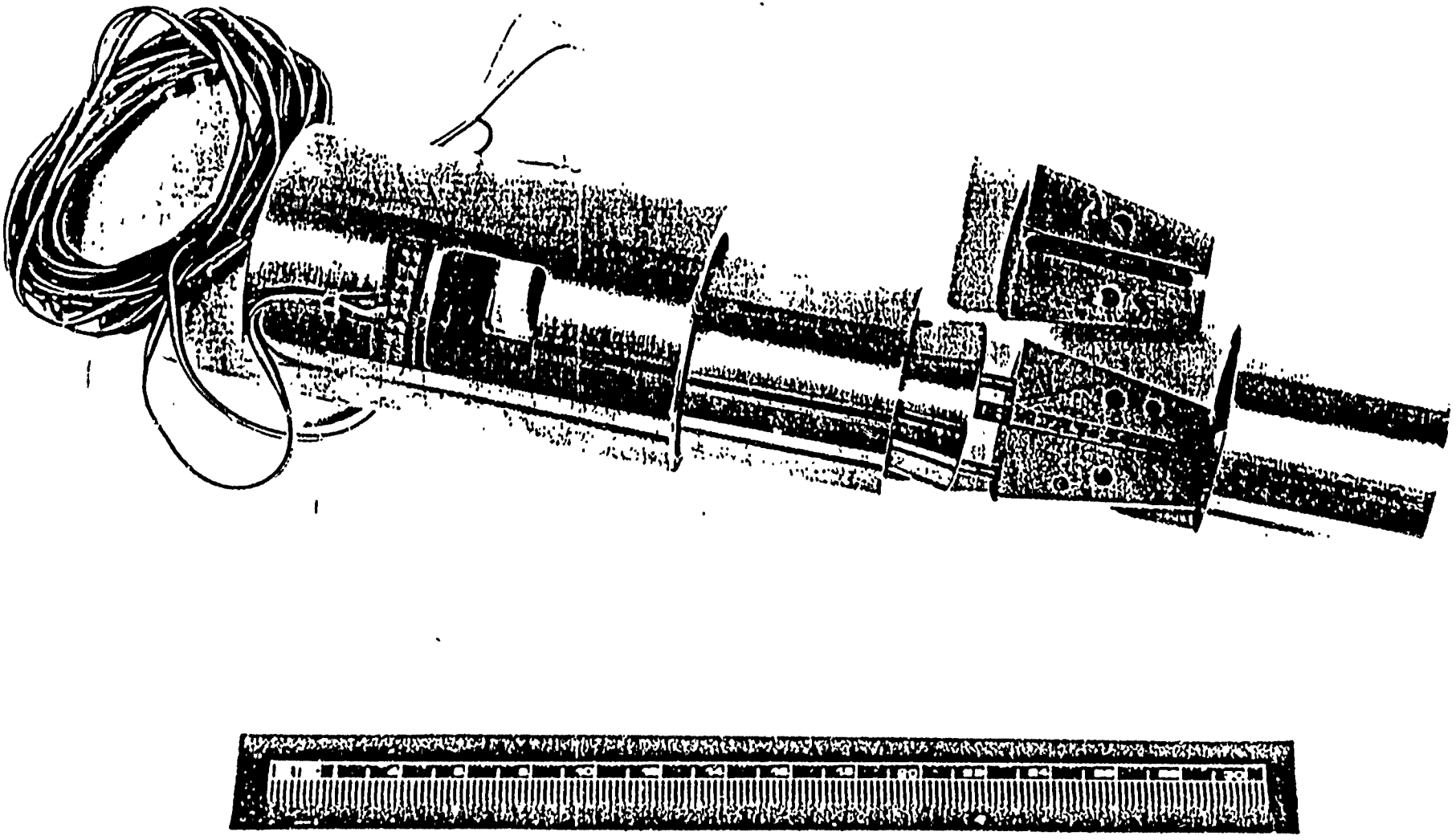

Figure 6. 'Celanese' compression fixture.

transverse normal stresses are applied simultaneously, strength coupling would be manifested by a change of biaxial longitudinal strength from the corresponding uniaxial longitudinal strength. In the limiting case, if the biaxial strengths are the same as the uniaxial strength, then the composite strength can be characterized by a non-interacting failure criterion such as the maximum stress failure criterion. Along these lines, we may think of the biaxial test as a test to identify strength coupling deviation from the maximum stress failure criterion. In order to definitively measure the existence of such deviations experimentally, the biaxial ratio (β in Figure 4f) must be chosen such that the measured deviation (if any) is statistically significant over the usual material scatter. The importance of using an optimal biaxial ratio β is illustrated in Figure 7(a) where the maximum stress failure criterion and a second-order polynomial failure criterion are illustrated. An optimal biaxial ratio is along the radial direction where the difference between the two failure criterion is maximum. The derivation of methods to calculate this optimal biaxial ratio is presented in Reference (5). A simplified (but approximate) estimation of the biaxial ratio can be observed by representing the failure criteria in normalized form in Figure 7b. In the normalized failure surfaces, the maximum stress criterion is a square and the second-order tensor polynomial with $F_{12} = 0$ is a circle. We can easily observe that the largest differences occur at the corners or equivalently at $\beta = X_1/X'_2$. The degree of such an approximation deteriorates when $F_{12} \neq 0$. Using this approximation for the worse case, (liquid at 100°C) $\beta \approx -5$; whereas by rigorous calculation (Reference 5) $\beta = -10$. We used $\beta = -10$ in our biaxial tests.

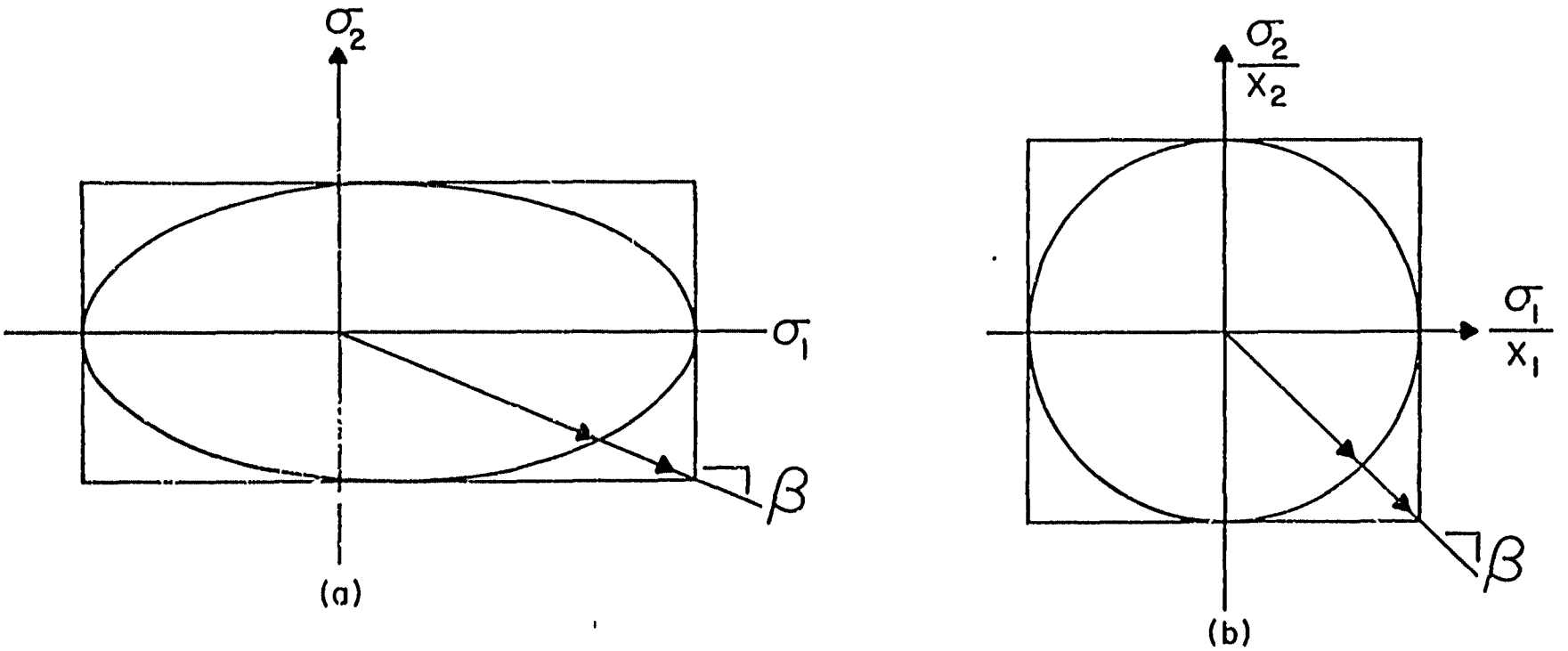

Figure 7. Interpretation of optimal biaxial ratio β

(a) in the normal stress space
(b) in the normalized normal stress space

The test results of the six guiding experiments are shown respectively in Tables 2 to 5 and in Figures 8 to 13. On the left of each figure are the stress-strain responses and on the right are the corresponding ultimate strengths for the different moisture exposure conditions.

REPRESENTATION OF THE MOISTURE-DEGRADED FAILURE SURFACE

Representation of the failure surface in terms of a tensor polynomial for a failure surface at a given physical state has two operational conveniences. The first is the possibility of a systematic experimental measurement which we have undertaken in this investigation. The second is a clear identification of material coefficients. When failure strength is represented in terms of stress, it is physically inconsistent, since stress is in fact the input or the independent variable. In the tensor polynomial representation, the strength tensors F_i, F_{ij} have the units of $[\text{Stress}]^{-1}$ and $[\text{Stress}]^{-2}$ and have the same constitutive consistency as moduli to strain. We can therefore characterize the moisture-degraded state in terms of the strength tensors F_i, F_{ij}. That is if $F_i(\Theta)$, $F_{ij}(\Theta)$ are known, where Θ is a variable characterizing the moisture absorption, then the failure surface at those states is uniquely determined by Equation (1). In this problem we define Θ as:

$$\Theta = \text{Equilibrium Moisture Content} - M_m \text{ (matrix moisture)} \qquad (2)$$

$$\Theta = M_m (T,C)$$

where T is the temperature and C is the moisture concentration.

Table 2

Longitudinal Ultimates

GPa x 145 = Ksi

	DRY, 23°C		52% RH, 23°C		Liquid H_2O, 23°C		Liquid H_2O, 100°C	
Tensile	Stress (GPa)	Strain (%)	Stress (GPa)	Strain (%)	Stress (GPa)	Strain (%)	Stress (GPa)	Strain (%)
	1.44	1.83	1.42	1.89	1.26	1.73	1.27	1.66
	1.39	1.88	1.36	1.87	1.22	1.67	1.22	1.72
	1.38	1.75	1.34	1.73	1.18	1.52	1.16	1.63
	1.35	1.77	1.30	1.77	1.16	1.69	1.08	1.52
	1.31	1.69	1.28	1.79	1.12	1.58	1.02	1.44
$\bar{X}_1$	1.37	1.78	1.34	1.81	1.19	1.64	1.15	1.59
S_1	0.05	0.07	0.09	0.07	0.05	0.09	0.10	0.11
Compression								
	-0.198	-0.555	-0.185	-0.471	-0.145	-0.321	-0.128	-0.331
	-0.194	-0.475	-0.181	-0.422	-0.141	-0.335	-0.111	-0.259
	-0.187	-0.440	-0.171	-0.415	-0.121	-0.276	-0.110	-0.315
	-0.186	-0.492	-0.161	-0.365	-0.120	-0.314	-0.107	-0.281
	-0.173	-0.390	-0.146	-0.349	-0.101	-0.283	-0.080	-0.216
$\bar{X}_1$	-0.188	-0.470	-0.169	-0.404	-0.126	-0.306	-0.107	-0.280
S_1	0.010	0.061	0.016	0.047	0.018	0.025	0.017	0.046

Table 3

Transverse Ultimates

(MPa) (0.145) = Ksi

	DRY, 23°C		52% RH, 23°C		Liquid H_2O, 23°C		Liquid H_2O, 100°C	
Tensile	Stress (MPa)	Strain (%)	Stress (MPa)	Strain (%)	Stress (MPa)	Strain (%)	Stress (MPa)	Strain (%)
	9.3	0.19	8.7	0.18	4.8	0.11	4.4	0.10
	8.2	0.15	7.9	0.15	4.1	0.09	3.8	0.09
	7.5	0.15	7.5	0.14	3.9	0.09	3.7	0.08
	7.2	0.13	6.9	0.14	3.5	0.08	3.1	0.08
	5.9	0.10	6.0	0.12	3.2	0.07	2.8	0.07
$\bar{X}_2$	7.6	0.14	7.4	0.15	3.9	0.09	3.6	0.08
S_2	1.3	0.03	1.0	0.02	0.6	0.01	0.6	0.01
Compression								
	-34.5	-0.88	-33.3	-0.72	-26.1	-0.53	-24.5	-0.6.
	-33.1	-0.65	-31.0	-0.84	-23.3	-0.52	-23.1	-0.56
	-31.2	-0.63	-28.9	-0.68	-23.2	-0.42	-22.3	-0.44
	-30.0	-0.56	-26.8	-0.59	-20.3	-0.44	-21.3	-0.50
	-27.9	-0.55	-25.1	-0.51	-19.5	-0.45	-19.5	-0.38
$\bar{X}'_2$	-31.3	-0.65	-29.0	-0.67	-22.5	-0.47	-22.1	-0.58
S'_2	2.6	0.13	3.3	0.13	2.6	0.05	19.0	0.09

Table 4

Shear Ultimates

(MPa) (0.145) = Ksi

	DRY, 23°C		52% RH, 23°C		Liquid H_2O, 23°C		Liquid H_2O, 100°C	
	Stress (MPa)	Strain (%)	Stress (MPa)	Strain (%)	Stress (MPa)	Strain (%)	Stress (MPa)	Strain (%)
	29.3	2.52	28.0	2.45	15.8	1.21	15.5	1.05
	28.5	2.05	27.3	2.98	14.9	1.12	15.0	1.23
	27.3	2.07	26.7	2.15	14.5	1.03	14.5	1.12
	26.0	1.75	25.8	2.02	12.7	0.95	11.8	0.95
	24.1	1.51	24.6	1.75	11.3	0.93	11.1	0.78
$\bar{X}_6$	27.0	1.98	26.5	2.27	13.8	1.05	13.6	1.03
S_6	2.1	0.38	1.3	0.47	1.8	0.12	2.0	0.17

Table 5

Biaxial Ultimates

(GPa) (145) = Ksi

DRY, 23°C		52% RH, 23°C		Liquid H_2O, 23°C		Liquid H_2O, 100°C	
Stress (GPa)	Strain (%)	Stress (GPa)	Strain (%)	Stress (GPa)	Strain (%)	Stress (GPa)	Strain (%)
1.89	2.21	1.77	2.05	1.40	1.66	1.27	1.45
1.79	2.11	1.66	2.08	1.30	1.75	1.02	1.25
1.68	1.90	1.53	1.82	1.35	1.71	1.15	1.35
1.62	1.95	1.65	1.98				
1.57	1.88	0.12	0.14				
$\bar{\tilde{\sigma}}_1^*$ 1.71	2.01						
$\tilde{S}_1^*$ 0.13	0.14						

$$\text{Biaxial Ratio} = \frac{\text{Longitudinal}}{\text{Transverse}} \quad \frac{\tilde{\sigma}_1}{\tilde{\sigma}_2} = \frac{10}{-1}$$

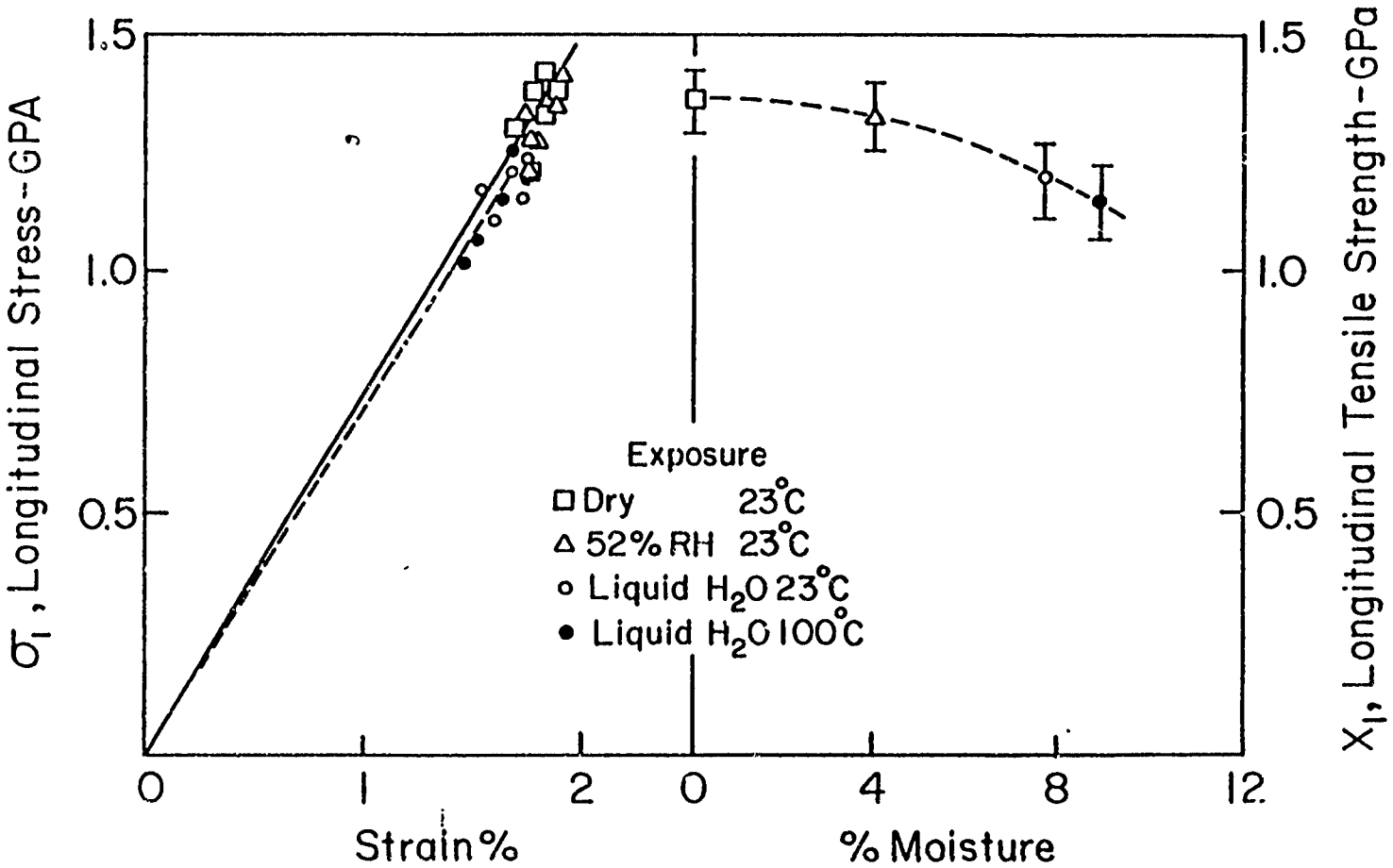

Figure 8. Longitudinal tensile behavior of K-49 at different environmental conditions. Left, average stress-strain responses and failure points; right, tensile strength degradation as a function of moisture contents (GPa x 145 = Ksi).

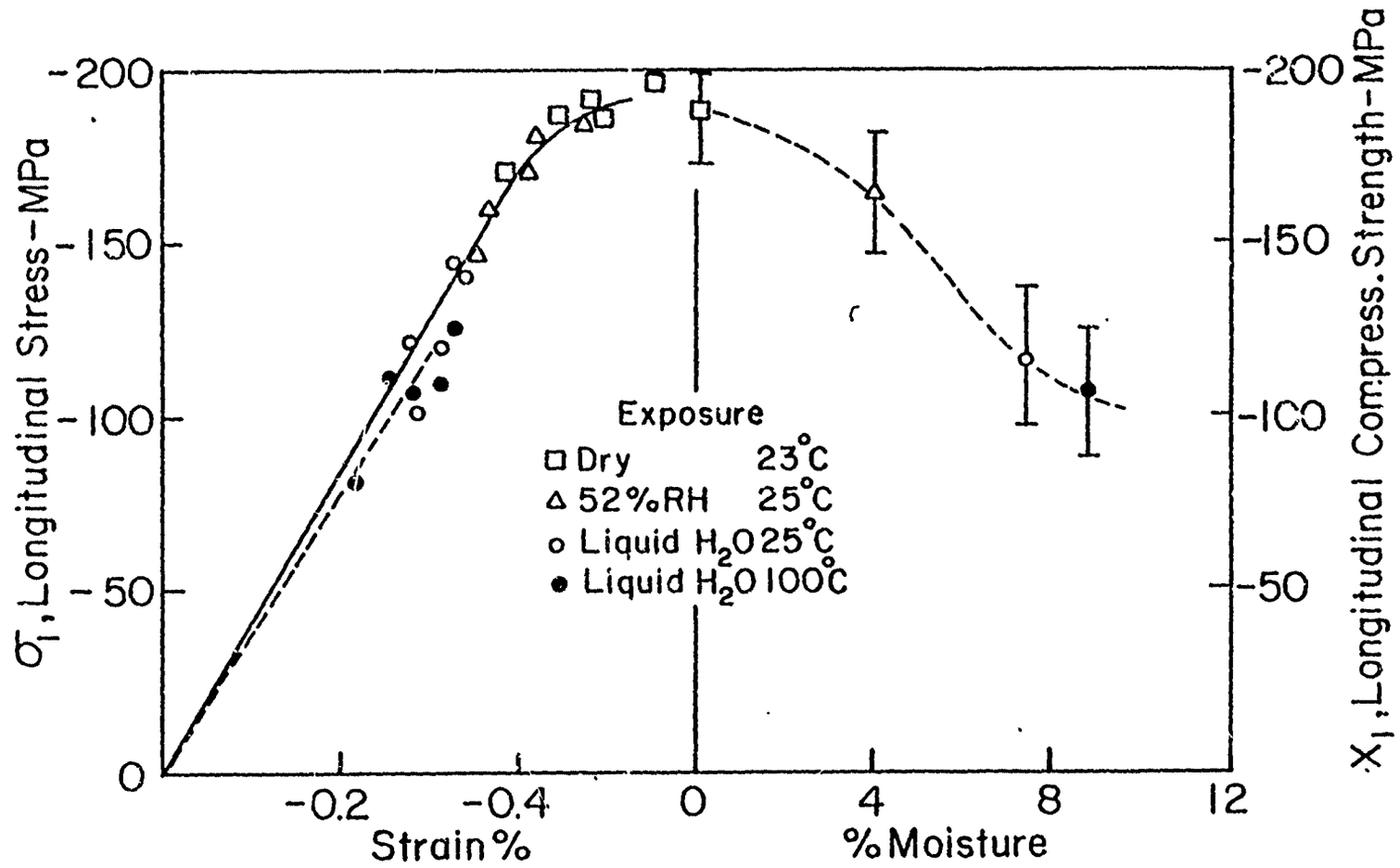

Figure 9. Longitudinal compressive behavior of K-49 at different environmental conditions. Left, average stress-strain responses and failure points; right, longitudinal compressive strength degradation as a function of moisture contents (MPa x .145 = Ksi).

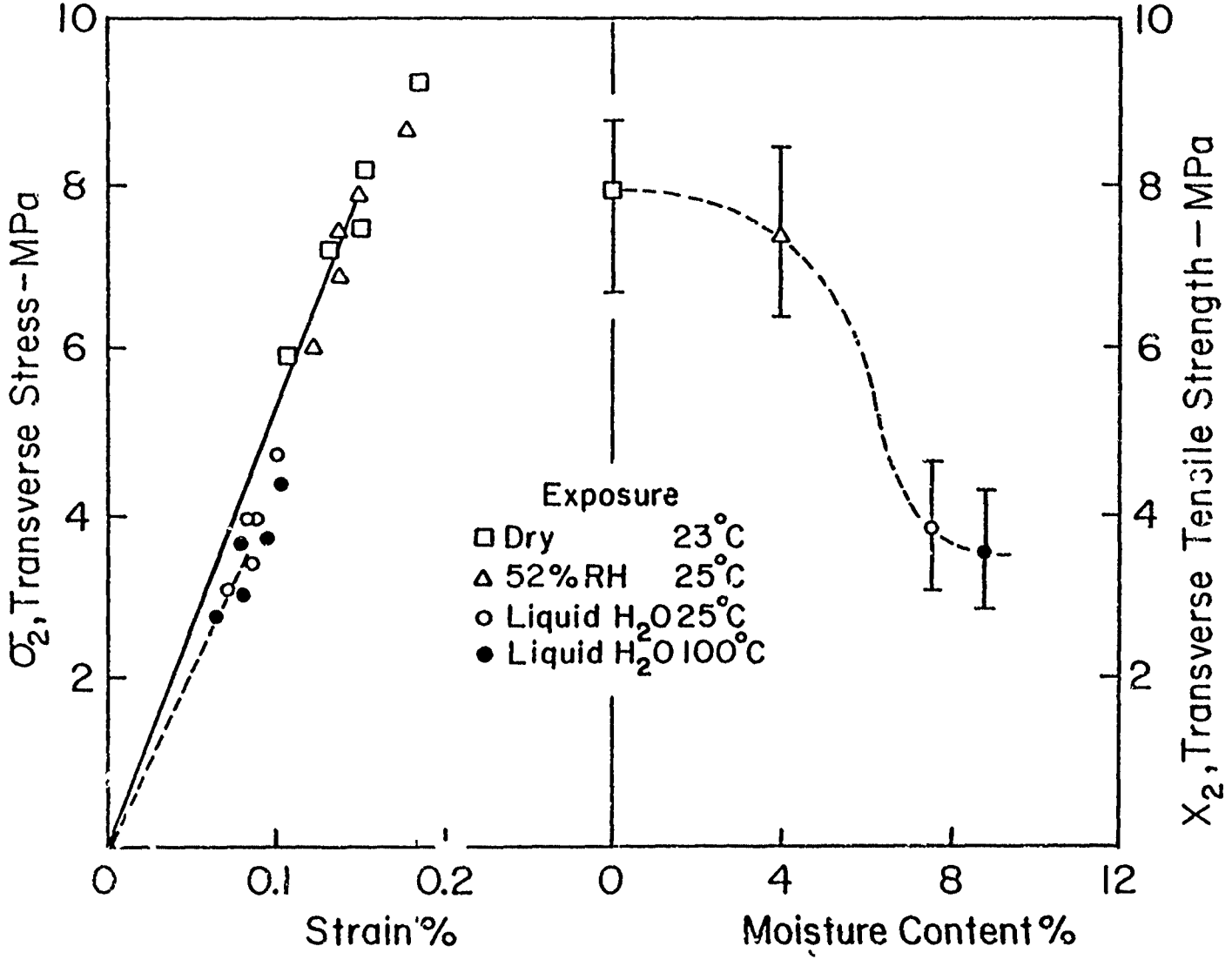

Figure 10. Transverse tensile behavior of K-49 at different environmental conditions. Left, average stress-strain responses and failure points; Right, tran. .erse tensile strength as a function of moisture contents (MPa x .145 = Ksi).

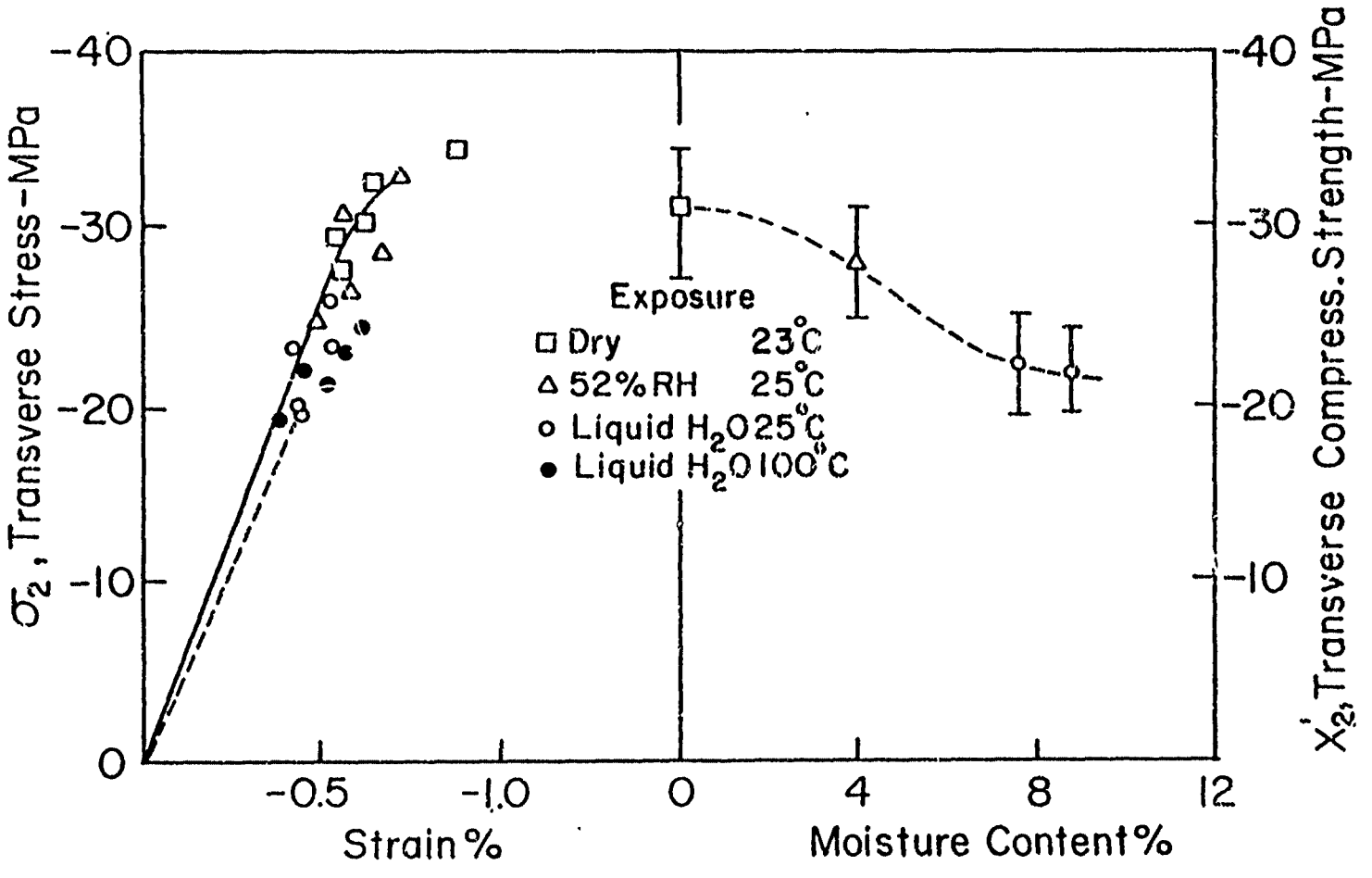

Figure 11. Transverse compressive behavior of K-49 at different environmental conditions. Left, average stress-strain responses and failure points; right, transverse compressive strength as a function of moisture contents (MPa x .145 = Ksi).

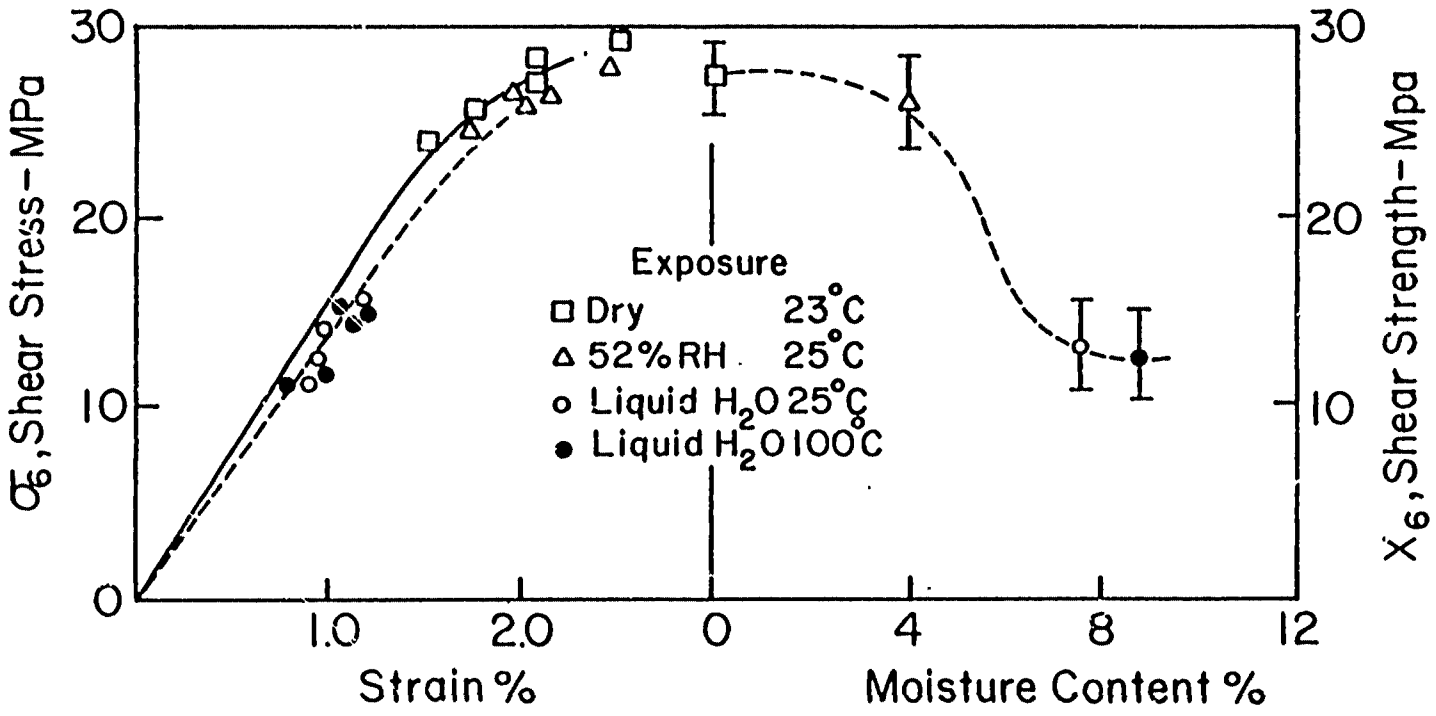

Figure 12. Shear behavior of K-49 at different environmental conditions. Left, average stress-strain responses and failure points; right, shear strength as a function of moisture contents (MPa x .145 = Ksi).

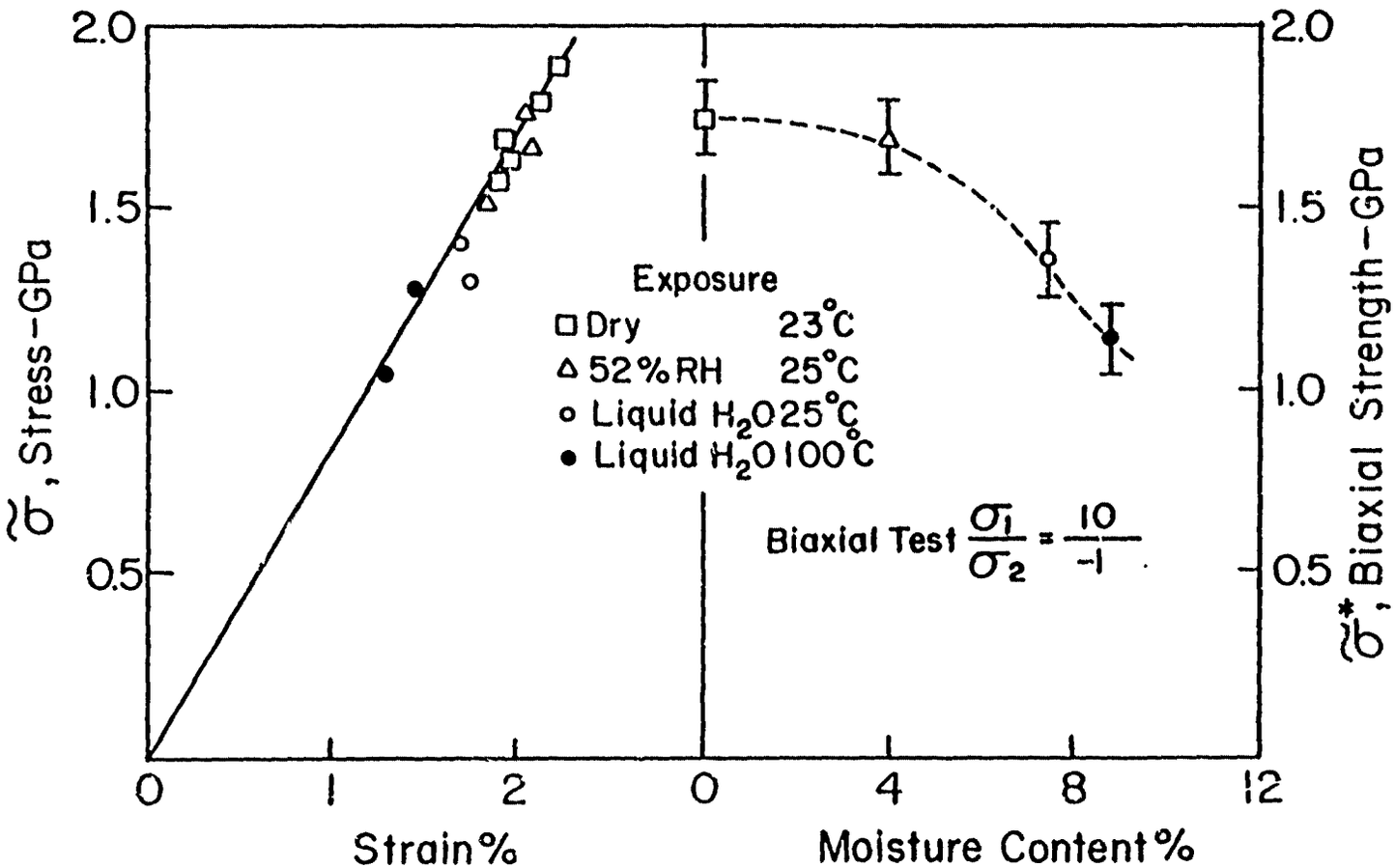

Figure 13. Biaxial (longitudinal and transverse) loading behavior of K-49 at different environmental conditions. Left, average stress-strain response in the longitudinal direction and failure points measuring strength coupling; right, biaxial strength as a function of moisture contents (MPa x .145 = Ksi).

To obtain $F_1(\Theta)$, $F_{ij}(\Theta)$, we need to determine:

$$F_i(\Theta) = \frac{1}{X_i(\Theta)} - \frac{1}{X_i'(\Theta)}$$

$$F_{ij}(\Theta) = \frac{1}{X_i(\Theta)\ X_i'(\Theta)} \qquad (3)$$

where X_i and X_i' refer to the positive and negative strength values measured for condition Θ if the failure surface can be represented as a 2nd-order surface, i.e. an ellipsoid. To examine the latter point, we presented the strength measurements in the stress space in Figures 14 and 15. In Figures 14 and 15, a second-order polynomial (the ellipse) is fitted to the axis crossings. In addition, the maximum stress criterion (the rectangle) is also represented for comparison. Cursory inspection of Figure 14 reveals that the maximum stress criterion is a poor representation of the biaxial loading condition. On the other hand, a second-order polynomial does not sufficiently provide a reasonable representation. The reason for this is that there are drastic differences between tensile and compressive strengths for Kevlar-49 composites. Such large strength differences displace the center of the ellipse far away from the origin, giving rise to the unreasonable prediction that both in the first and fourth stress quadrants (Figure 14), biaxial loading increases the uniaxial strengths. In order to eliminate such objections, a failure criterion containing terms higher than second-order is required. The methodology for evaluating third-order terms for the tensor polynomial has been discussed in Ref. 4.

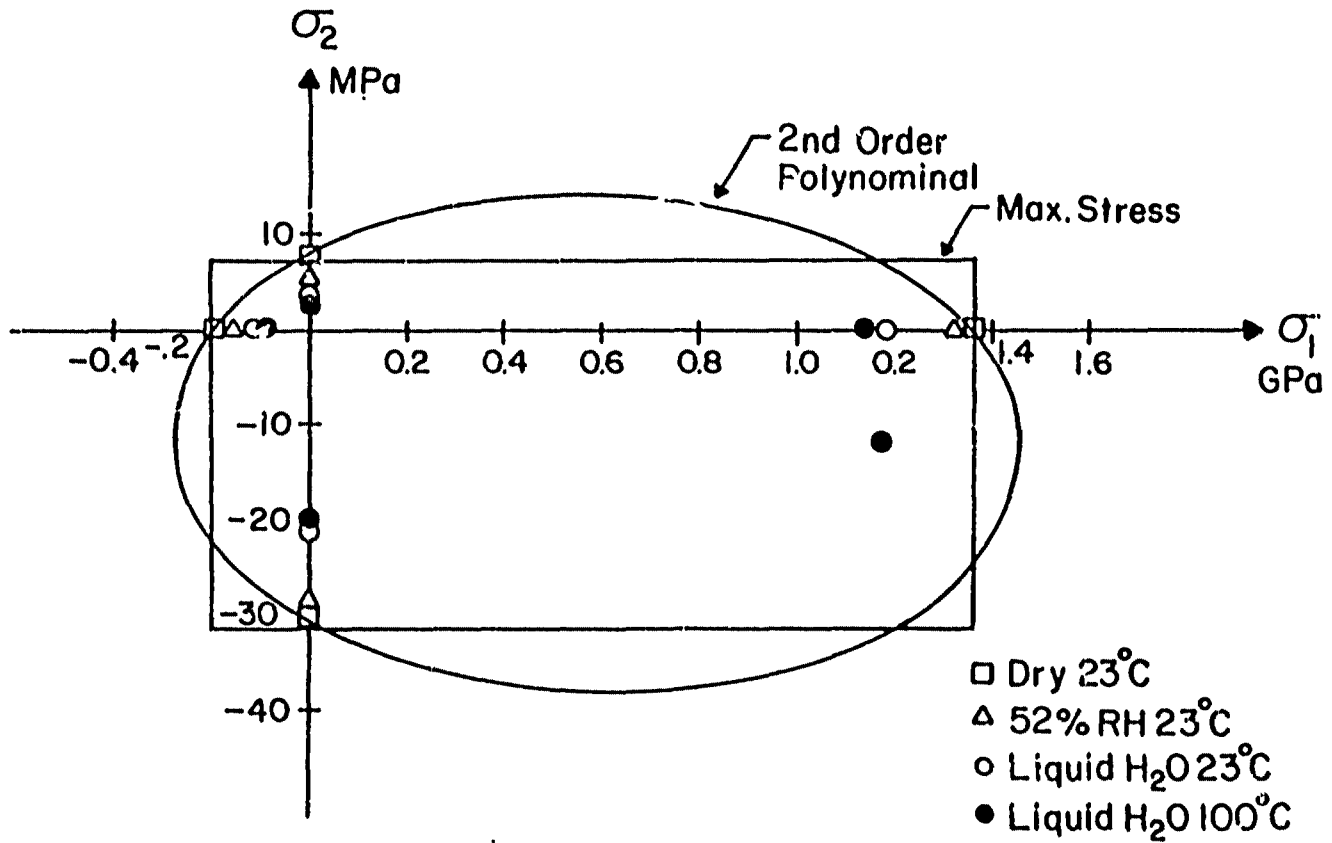

Figure 14. Failure data in the σ_1-σ_2 space. Second-order polynomial and maximum stress criterion are fitted to the dry state at 23°C. Necessity for third-order tensor polynomial is indicated because of the large differences between tensile and compressive strength.

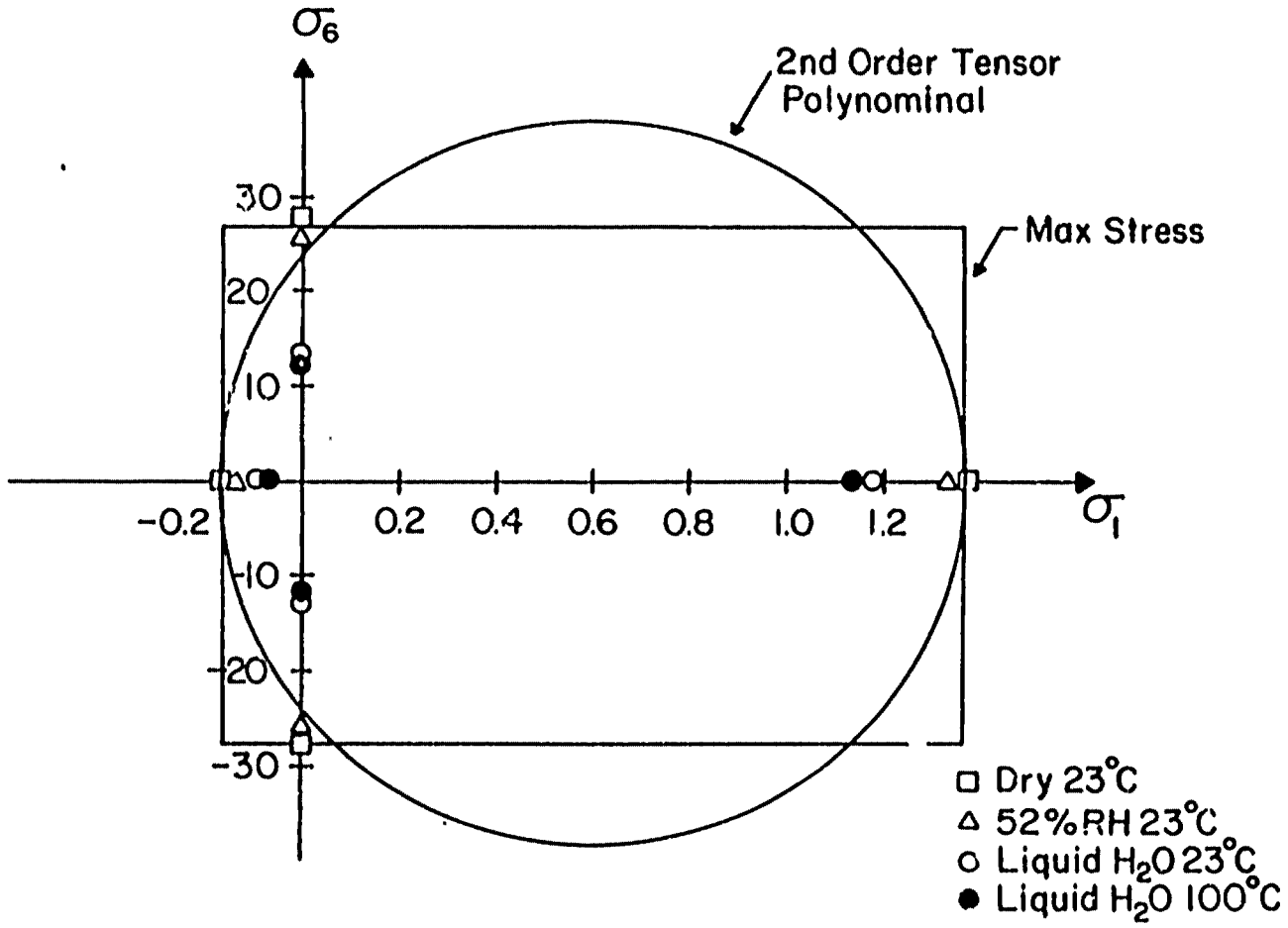

Figure 15. Failure data in the σ_1-σ_6 space. Second-order tensor polynomial and maximum stress criterion fitted to the dry state at 23°C.

The experimental evaluation of the higher order terms involves additional measurements which are beyond the scope of this investigation.

Another consequence of the large differences between tensile and compressive strengths is that it is difficult to assess the effect of environment from the failure strength in stress space (Figures 14 and 15). This difficulty can be overcome by examining the effect of water and temperature in the normalized strength space where the controlled dry state at room temperature is used as the reference state. Such a representation is given in Figure 16. An ellipse with $F_{12} = 0$ would appear as a circle in the normalized space. We note from Figure 16 that the effect of moisture and temperature on the longitudinal tensile property is small compared to that on the compressive and transverse properties. As a consequence of such differences in degree of degradation, the center of the failure surface is shifted, accompanied by a general distortion. Analytical representation of such changes clearly requires 3rd-order terms. Since adequate experimental results are not available for calculation of the 3rd-order terms, calculation of the 2nd-order terms in F_i, F_{ij} can only serve to produce misleading conclusions. Four additional biaxial experiments to measure F_{112}, F_{221}, F_{166} and F_{266} are recommended.

CONCLUSION

The moisture absorption kinetics for Kevlar 49 epoxy have been measured for four environmental conditions. The strength degradation for the composite has been systematically measured by six experiments for each of the four states. The tensor polynomial strength coefficients

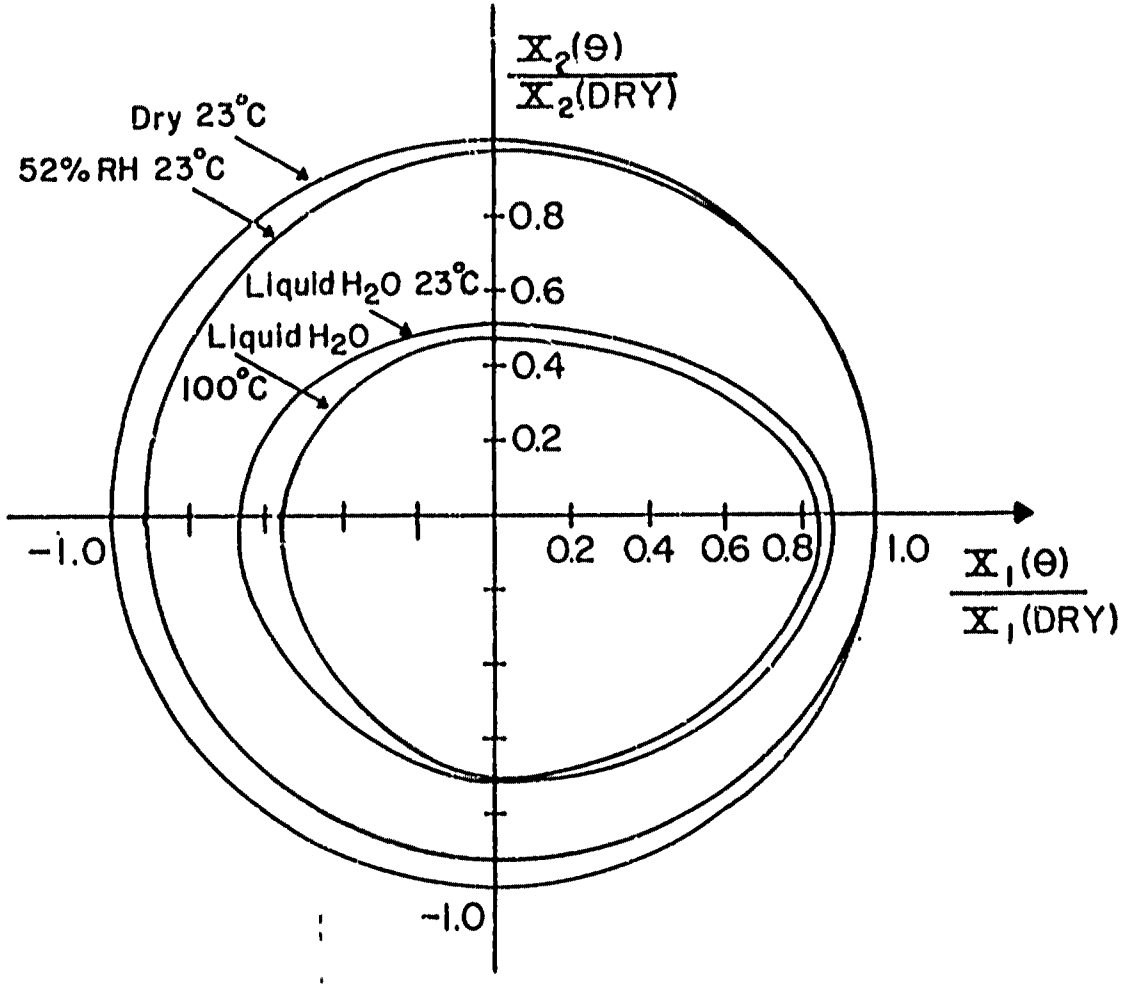

Figure 16. Effect of environment on the strength surface in the space normalized by the dry state.

are generalized to represent the strength degradation for the moisture-absorbed states.

Due to the big difference between tensile and compressive strengths for Kevlar 49 composites, analytical representation of the failure surface requires a third-order tensor polynomial. Four additional biaxial experiments are needed to provide the necessary data. Different degrees of strength degradation in the fiber-controlled vs. matrix-controlled strength causes the failure surface to shift and deform. This should also be characterized by a third-order tensor polynomial.

REFERENCES

1. C. E. Browning, G. E. Husman and J. M. Whitney, "Moisture Effects in Epoxy Matrix Composites", Composite Materials Testing and Design, ASTM, STP 617, 1976.

2. G. S. Springer and C. H. Shen, "Effect of Moisture and Temperature on Tensile Strength of Composite Materials", Journal of Composite Materials, 11, 2 (1977).

3. N. J. Abbott, J. G. Donovan, M. M. Schoppee and J. Skelton, "Some Mechanical Properties of Kevlar and Other Heat Resistant, Nonflammable Fibers, Yarns and Fabrics", Air Force Materials Laboratory, AFML-TR-74-65, 1975.

4. E. M. Wu, "Phenomenological Anisotropic Failure Criterion", Treatise on Composite Materials, Broutman, Krock and Sendeckyj, Eds., Academic Press, New York, 1973.

5. E. M. Wu, "Optimal Experiments for Measurement of Failure Tensors", Journal of Composite Materials, 6, 473 (1972).

6. T. T. Chiao, E. S. Jessop and H. A. Newey, "A Moderate Temperature Curable Epoxy for Advanced Composites", UCRL Preprint 76126, October, 1974.

APPENDIX

Specimen Fabrication

A summary of specimen fabrication procedures is presented here. Samples for testing were provided by the sponsor, the U. S. Army Materials and Mechanics Research Center. Specimen geometries were of two major types: cylindrical tubes and flat plates. The majority of the tubes fabricated were nominally 1" I.D. specimens of approximately 0.05" wall thickness, with a nominal 90° wrap angle. All samples were wet wound on an En-Tech Model 830 filament winder using Kevlar type 969 roving (4560 denier) with the XD7818/Jeffamine T403 epoxy system. The specimens were wound in one direction only; that is, the winder feed transversed the sample in one direction, halted, returned to its initial winding location, and winding was continued. This method was employed instead of a "back and forth" winding pattern in order to eliminate fiber crossover points in alternate layers. A total of four layers of Kevlar was employed. The nominal 90° samples were actually wound at 87.7° to the axis of the tubes due to the requirements and limitations of the filament winding process. Winding tension employed was 1400 grams. In addition to the 90° specimens, other tubes including a quantity of $\pm$ 10° specimens were prepared in order to approximate axially-reinforced cylinders. Winding tension in this case was 1600 grams.

Unidirectional flat-plate specimens of the same material were prepared using the En-Tech winder. In this case, a "flat" mandrell 26" in length was employed and four 8" x 8" specimen plates were made simultaneously, two plates being produced on each side of the mandrel by

spacing winding zones along the mandrel's length. Plate thickness was nominally 0.06". All samples were B-staged on the mandrels using IR heating and then post-cured in an oven for 2 hours at 100°C. Surface appearance of the completed samples was typical of as-wound Kevlar/epoxy, i.e., Kevlar fibrillation at the specimen surface when covered by epoxy yielded a rather grainy surface texture. Details of the resin chemistry can be found in Reference (6).

DISTRIBUTION LIST

No. of Copies	To
1	Office of the Director, Defense Research and Engineering, The Pentagon, Washington, D. C. 20301
12	Commander, Defense Documentation Center, Cameron Station, Building 5, 5010 Duke Street, Alexandria, Virginia 22314
1	Metals and Ceramics Information Center, Battelle Columbus Laboratories, 505 King Avenue, Columbus, Ohio 43201
	Deputy Chief of Staff, Research, Development, and Acquisition, Headquarters Department of the Army, Washington, D. C. 20310
1	ATTN: DAMA-ARZ
2	Dr. J. I. Bryant
	Commander, Army Research Office, P. O. Box 12211, Research Triangle Park, North Carolina 27709
1	ATTN: Information Processing Office
2	Dr. J. Hurt
1	Dr. G. Mayer
1	Dr. D. Squire
	Commander, U. S. Army Materiel Development and Readiness Command, 5001 Eisenhower Avenue, Alexandria, Virginia 22333
1	ATTN: DRCLDC, Mr. R. Zentner
	Commander, U. S. Army Electronics Research and Development Command, Fort Monmouth, New Jersey 07703
1	ATTN: DRSEL-GG-DD
1	DRSEL-GG-DM
	Commander, U. S. Army Missile Research and Development Command, Redstone Arsenal, Alabama 35809
1	ATTN: Technical Library
2	DRDMI-RUM, Mr. H. E. Dedman
	Commander, U. S. Army Armament Research and Development Command, Dover, New Jersey 07801
2	ATTN: Technical Library
1	DRDAR-SCM, J. D. Corrie
	Commander, U. S. Army Natick Research and Development Command, Natick, Massachusetts 01760
1	ATTN: Technical Library
	Commander, U. S. Army Aviation Research and Development Command, P.O. Box 209, St. Louis, Missouri 63166
1	ATTN: Technical Library
	Commander, U. S. Army Satellite Communications Agency, Fort Monmouth, New Jersey 07703
1	ATTN: Technical Document Center

No. of Copies	To
	Commander, White Sands Missile Range, New Mexico 88002
1	ATTN: STEWS-WS-VT
	Commander, Aberdeen Proving Ground, Maryland 21005
1	ATTN: STEAP-TL, Bldg. 305
	Commander, Frankford Arsenal, Philadelphia, Pennsylvania 19137
1	ATTN: Library, M1300, Bl. 51-2
	Commander, Harry Diamond Laboratories, 2800 Powder Mill Road, Adelphi, Maryland 20783
2	ATTN: Technical Information Office
2	Dr. S. Y. Lee
	Commander, Picatinny Arsenal, Dover, New Jersey 07801
1	ATTN: SARPA-RT-S
2	SARPA-FR-M-D, PLASTEC, Mr. H. Pebly
1	SARPA-FR-M-D, PLASTEC, Mr. A. Slobodzinski
1	SMUDA-FR-A, Mr. W. Tanner
	Commander, Redstone Scientific Information Center, U. S. Army Missile Command, Redstone Arsenal, Alabama 35809
4	ATTN: DRDMI-TB
	Chief, Benet Weapons Laboratory, LCWSL, USA ARRADCOM, Watervliet, New York 12189
1	ATTN: DRDAR-LCB-TL
	Commander, U. S. Army Foreign Science and Technology Center, 220 7th Street, N. E., Charlottesville, Virginia 22901
1	ATTN: Military Tech, Mr. Marley
	Director, Eustis Directorate, U. S. Army Air Mobility Research and Development Laboratory, Fort Eustis, Virginia 23604
2	ATTN: Mr. W. Figge
1	Dr. R. L. Foye
	Commander, USACDC Air Defense Agency, Fort Bliss, Texas 79916
1	ATTN: Technical Library
	Technical Director, Human Engineering Laboratories, Aberdeen Proving Ground, Maryland 21005
1	ATTN: Technical Reports Office
	Commander, U. S. Army Engineering Research and Development Laboratory, Fort Belvoir, Virginia 22060
1	ATTN: Mr. S. Goldfein
	Commander, U. S. Army Medical Bioengineering Research and Development Laboratory, Fort Detrick, Maryland 21701
1	ATTN: Dr. C. Wade, SGRD-UBF
	Chief of Naval Research, Arlington, Virginia 22217
1	ATTN: Code 471

No. of Copies	To
1	Dr. D. H. Kaelble, Science Center, Rockwell International, Thousand Oaks, California 91360
1	Dr. B. W. Rosen, Materials Science Corporation, Blue Bell, Pennsylvania 19422
	Defense Research Establishment Office, Sheelay Bay, Ottawa, Ontario KIA 024
1	ATTN: Mr. H. L. Nash
	Defence Standard Laboratories, Dept. of Supply, P.O. Box 50, Ascot Vale 3032, Victoria, Australia
1	ATTN: Dr. D. Pinkerton
1	Dr. G. George
	Director, Army Materials and Mechanics Research Center, Watertown, Massachusetts 02172
2	ATTN: DRXMR-PL
1	DRXMR-AG-MD
2	DRXMR-TM(Dr. E. Lenoe)
1	DRXMR-RC(Ms. M. Roylance)
1	DRXMR-RC(Mr. N. Tessier)
9	DRXMR-RC(Mr. J. Gassner)
	Commander, US Army Aeromedical Research Unit, P.O. Box 577, Fort Rucker, Alabama 36460
1	ATTN: Technical Library
	Commander, Naval Air Engineering Center Lakehurst, New Jersey 08733
1	ATTN: Technical Library, Code 115
	Director, Structural Mechanics Research Office of Naval Research, 800 North Quincy Street Arlington, VA 22203
1	ATTN: Dr. N. Perrone
	Naval Air Development Center, Aero. Materials Department, Warminster, Pennsylvania 18974
1	ATTN: J. Viglione
	David Taylor Naval Ship R&D Laboratory Annapolis, Maryland
1	ATTN: Dr. H.P. Chu
	US Army Aviation Training Library, Fort Rucker, Alabama 36360
1	ATTN: Bldg. 5906-5907
	US Army Engineer School, Ft. Belvoir, Virginia 22060
1	ATTN: Technical Library

No. of Copies	To
	Office of Naval Research, Boston Branch, 495 Summer Street, Boston, Massachusetts 02210
1	ATTN: Dr. L. H. Peebles
	Naval Research Laboratory, Washington, D. C. 20375
2	ATTN: Dr. W. B. Moniz, Code 6120
2	Dr. I. Woloch, Code 8433
3	Dr. W. D. Bascom, Code 6170
2	Dr. L. B. Lockhart, Jr., Code 6120
	Commander, Naval Air Systems Command, Washington, D. C.
2	ATTN: Mr. C. Bersch
	Commander, Naval Surface Weapons Center, White Oak, Silver Spring, Maryland 20910
1	ATTN: Dr. J. M. Augl
	Air Force Office of Scientific Research (NC), Bldg. 410, Bolling Air Force Base, Washington, D. C. 20332
1	ATTN: Dr. D. R. Ulrich
	Air Force Materials Laboratory, Wright-Patterson Air Force Base, Ohio 45433
1	ATTN: Dr. S. W. Tsai
1	Dr. N. J. Pagano
1	Dr. H. T. Hahn
1	Dr. C. E. Browning
1	CAPT Dreal
1	Dr. I. Goldforb
1	Dr. E. Helminials
1	Dr. E. Reinhart
1	Dr. R. L. Van Deusen
	Air Force Flight Dynamics Laboratory, Wright-Patterson AFB, Ohio 45433
1	ATTN: Dr. J.C. Halpin
1	ATTN: Dr. G. P. Sendeckyj
	National Aeronautics and Space Administration, Washington, D. C. 20546
1	ATTN: Mr. B. G. Achhammer
	National Aeronautics and Space Administration, Lewis Research Center, 21000 Brookpark Road, Cleveland, Ohio 44135
2	ATTN: Dr. T. T. Serafini (49-1)
1	Professor D. F. Adams, Dept. of Mechanical Engineering, University of Wyoming, Laramie, Wyoming 82070
	Commander, US Army Tank-Automotive R&D Command Warren, MI 48090
1	ATTN: DRDTA-UL, Technical Library

No. of Copies	To
	US Army Engineer Waterways Experiment Station Vicksburg, Mississippi 39180
1	ATTN: Research Center Library
	Naval Underwater Systems Center, New London, Connecticut 06320
1	ATTN: R. Kasper
	National Bureau of Standards Washington, D.C. 20234
1	ATTN: Mr. J.A. Bennett
1	ATTN: Technical Library
	Commander, US Army Armament R&D Command Aberdeen Proving Ground, Maryland 21010
1	ATTN: DRDAR-QAC-E
	E.I. DuPont de Nemours & Company Wilmington, DE 19898
1	ATTN: Dr. Carl Zweben, Industrial Fibers Division, Textile Fibers Department
	Lockheed-Georgia Company 86 South Cobb Drive, Marietta,Georgia 30063
1	ATTN: Materials & Processes Engineering Department 71-11, Zone 54

Army Materials and Mechanics Research Center
Watertown, Massachusetts 02172
STRENGTH DEGRADATION OF ARAMID-FIBER/
EPOXY COMPOSITES
Edward M. Wu

Technical Report AMMRC TR 80-19, April 1980, 35 pp -
illus-table, D/A Project 1T162105AH84,
AMCMS Code 612105.11.H84

AB

UNCLASSIFIED
UNLIMITED DISTRIBUTION

Key Words

Composite materials
Aramid fiber
Kevlar
Epoxy Laminates
Degradation
Applied Mechanics
Mechanical Properties

The moisture absorption kinetics for Kevlar 49 epoxy have been measured for four environmental conditions. The strength degradation for the composite has been systematically measured by six experiments for each of the four states. The tensor polynomial strength coefficients are generalized to represent the strength degradation for the moisture absorbed states.

Due to the big difference between tensile and compressive strength for Kevlar 49 composites, analytical representation of the failure surface requires a third-order tensor polynomial. Four additional biaxial experiments are needed to provide the necessary data. The degree of fiber-controlled strength degradation is different from the degradation of matrix-controlled strength, which causes the failure surface to shift and deform. This shift should also be characterized by a third-order tensor polynomial.

Army Materials and Mechanics Research Center
Watertown, Massachusetts 02172
STRENGTH DEGRADATION OF ARAMID-FIBER/
EPOXY COMPOSITES
Edward M. Wu

Technical Report AMMRC TR 80-19, April 1980, 35 pp -
illus-table, D/A Project 1T162105AH84,
AMCMS Code 612105.11.H84

AB

UNCLASSIFIED
UNLIMITED DISTRIBUTION

Key Words

Composite materials
Aramid fiber
Kevlar
Epoxy Laminates
Degradation
Applied Mechanics
Mechanical Properties

The moisture absorption kinetics for Kevlar 49 epoxy have been measured for four environmental conditions. The strength degradation for the composite has been systematically measured by six experiments for each of the four states. The tensor polynomial strength coefficients are generalized to represent the strength degradation for the moisture absorbed states.

Due to the big difference between tensile and compressive strength for Kevlar 49 composites, analytical representation of the failure surface requires a third-order tensor polynomial. Four additional biaxial experiments are needed to provide the necessary data. The degree of fiber-controlled strength degradation is different from the degradation of matrix-controlled strength, which causes the failure surface to shift and deform. This shift should also be characterized by a third-order tensor polynomial.

Army Materials and Mechanics Research Center
Watertown, Massachusetts 02172
STRENGTH DEGRADATION OF ARAMID-FIBER/
EPOXY COMPOSITES
Edward M. Wu

Technical Report AMMRC TR 80-19, April 1980, 35 pp -
illus-table, D/A Project 1T162105AH84,
AMCMS Code 612105.11.H84

AB

UNCLASSIFIED
UNLIMITED DISTRIBUTION

Key Words

Composite materials
Aramid fiber
Kevlar
Epoxy Laminates
Degradation
Applied Mechanics
Mechanical Properties

The moisture absorption kinetics for Kevlar 49 epoxy have been measured for four environmental conditions. The strength degradation for the composite has been systematically measured by six experiments for each of the four states. The tensor polynomial strength coefficients are generalized to represent the strength degradation for the moisture absorbed states.

Due to the big difference between tensile and compressive strength for Kevlar 49 composites, analytical representation of the failure surface requires a third-order tensor polynomial. Four additional biaxial experiments are needed to provide the necessary data. The degree of fiber-controlled strength degradation is different from the degradation of matrix-controlled strength, which causes the failure surface to shift and deform. This shift should also be characterized by a third-order tensor polynomial.